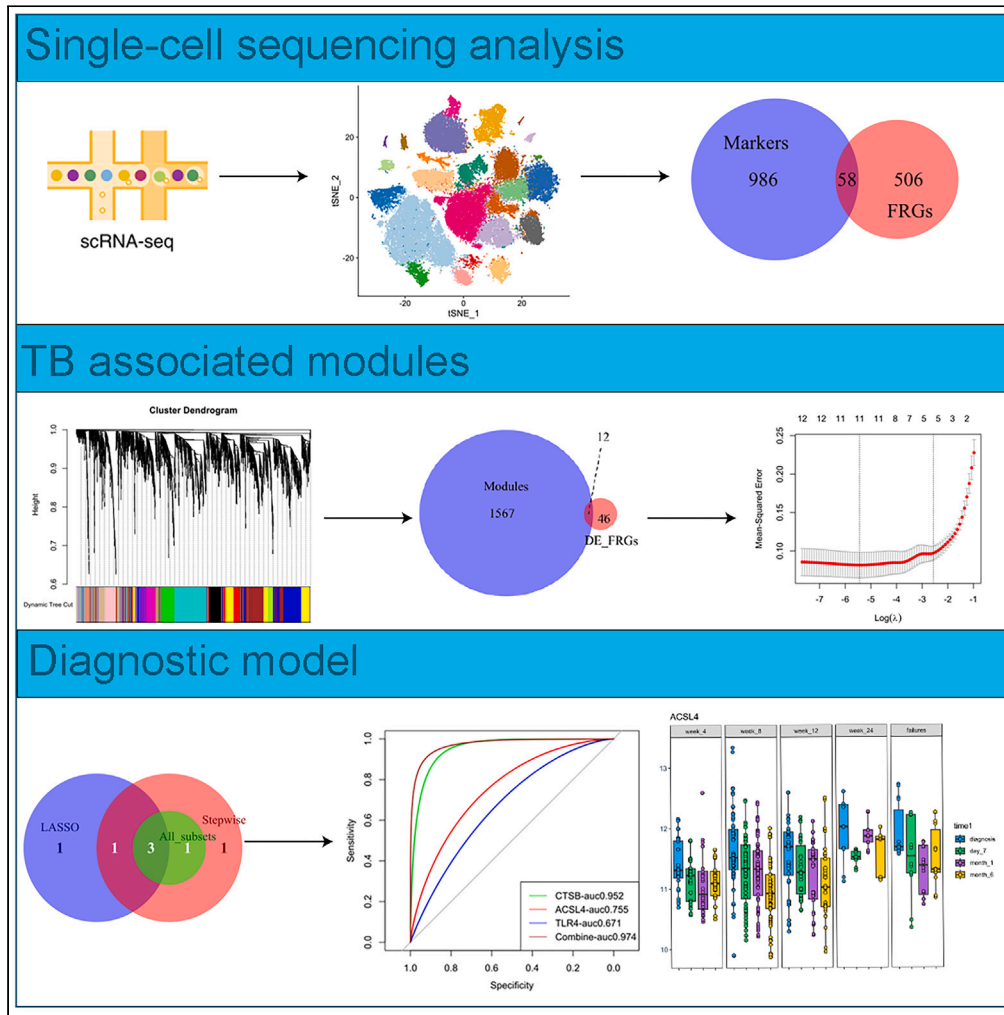


Article

# Identification of ferroptosis-related gene signature for tuberculosis diagnosis and therapy efficacy



Bingfen Yang, Fei Zhai, Zhimin Li, ..., Ruo Wang, Jing Jiang, Xiaoxing Cheng

jiang282000@139.com (J.J.)  
xcheng2@139.com (X.C.)

Highlights

A ferroptosis-related gene signature associated with TB was identified

The signature was associated with TB treatment efficacy

A potential biomarker for differentiating active TB from latent infection



## Article

## Identification of ferroptosis-related gene signature for tuberculosis diagnosis and therapy efficacy

Bingfen Yang,<sup>1,6</sup> Fei Zhai,<sup>1,6</sup> Zhimin Li,<sup>2</sup> Xinjing Wang,<sup>3</sup> Xianping Deng,<sup>4</sup> Zhihong Cao,<sup>1</sup> Yanhua Liu,<sup>1</sup> Ruo Wang,<sup>1</sup> Jing Jiang,<sup>5,\*</sup> and Xiaoxing Cheng<sup>1,7,\*</sup>

## SUMMARY

**Diagnosis of tuberculosis remains a challenge when microbiological tests are negative. Immune cell atlas of patients with tuberculosis and healthy controls were established by single-cell transcriptome. Through integrated analysis of scRNA-seq with microarray and bulk RNA sequencing data, a ferroptosis-related gene signature containing ACSL4, CTSB, and TLR4 genes that were associated with tuberculosis disease was identified. Four gene expression datasets from blood samples of patients with tuberculosis, latent tuberculosis infection, and healthy controls were used to assess the diagnostic value of the gene signature. The areas under the ROC curve for the combined gene signature were 1.000, 0.866, 0.912, and 0.786, respectively, in differentiating active tuberculosis from latent infection. During anti-tuberculosis treatment, the expression of the gene signature decreased significantly in cured patients with tuberculosis. In conclusion, the ferroptosis-related gene signature was associated with tuberculosis treatment efficacy and was a promising biomarker for differentiating active tuberculosis from latent infection.**

## INTRODUCTION

*Mycobacterium tuberculosis* (*Mtb*) is the etiological agent of tuberculosis (TB), one of the leading causes of death from an infectious disease.<sup>1</sup> It is estimated that about one-fourth of the world's population is infected with *Mtb*; most of them are in a state called latent TB infection (LTBI). Only 5%–10% infected people develop to active TB disease.<sup>1</sup> Host-immune-response-based tests, including interferon gamma (IFN- $\gamma$ ) release assay (IGRA) and tuberculin skin test (TST), are used for diagnosis of LTBI, but not recommended for diagnosis of active TB.<sup>2</sup> Despite extensive screening of blood transcriptional biomarkers, none of the signatures have sensitivity and specificity that meet WHO criteria of confirmatory test for TB.<sup>3</sup>

When *Mtb* enters lung through the aerosol route, it primarily infects alveolar macrophages.<sup>4</sup> *Mtb* establishes infection and survives intracellularly by evading host immune responses and hijacking molecular machinery in host cells.<sup>4–6</sup> Programmed and nonprogrammed cell death is critical for interaction between the well-adapted intracellular *Mtb* and the host cells it infects. Both apoptosis and autophagy are programmed cell death pathways that are found to be associated with a protective response, while cell death caused by pyroptosis, necroptosis, and ferroptosis might involve in *Mtb* infection.<sup>7,8</sup>

Unlike other types of programmed cell death, ferroptosis is caused by iron-dependent, overwhelming lipid peroxidation that leads to membrane rupture and cell death.<sup>9,10</sup> It is associated with inactivation of glutathione peroxidase-4 (GPX4) and reduced levels of glutathione.<sup>11,12</sup> GPX4 prevents lipid peroxidation and ferroptosis by converting toxic lipid hydroperoxides to nontoxic one.<sup>9</sup> Ferroptosis can be blocked by iron chelators and lipid peroxidation inhibitors.<sup>9</sup>

Ferroptosis contributes to *Mtb* pathogenesis and dissemination. Macrophages infected by *Mtb* undergoes ferroptosis, leading to dissemination of infection.<sup>11</sup> Mice deficient for *Gpx4* showed increased lung necrosis and *Mtb* burdens upon experimental infection.<sup>13</sup> A protein tyrosine phosphatase A (PtpA) secreted by *Mtb* induces ferroptosis by targeting protein arginine methyltransferase 6 to suppress GPX4 expression and promotes pathogenicity and dissemination of *Mtb*.<sup>14</sup>

<sup>1</sup>Beijing Key Laboratory of New Techniques of Tuberculosis Diagnosis and Treatment, Institute of Tuberculosis Research, Senior Department of Tuberculosis, the Eighth Medical Center of PLA General Hospital, Beijing, China

<sup>2</sup>4th Division of Tuberculosis, Senior Department of Tuberculosis, the Eighth Medical Center of PLA General Hospital, Beijing, China

<sup>3</sup>Outpatient Department, Senior Department of Tuberculosis, the Eighth Medical Center of PLA General Hospital, Beijing, China

<sup>4</sup>Department of Laboratory Medicine, the Eighth Medical Center of PLA General Hospital, Beijing, China

<sup>5</sup>Institute of Research, Beijing Key Laboratory of Organ Transplantation and Immune Regulation, Senior Department of Respiratory and Critical Care Medicine, the Eighth Medical Center of PLA General Hospital, Beijing, China

<sup>6</sup>These authors contributed equally

<sup>7</sup>Lead contact

\*Correspondence: [jiang282000@139.com](mailto:jiang282000@139.com) (J.J.), [xcheng2@139.com](mailto:xcheng2@139.com) (X.C.)

<https://doi.org/10.1016/j.isci.2024.110182>



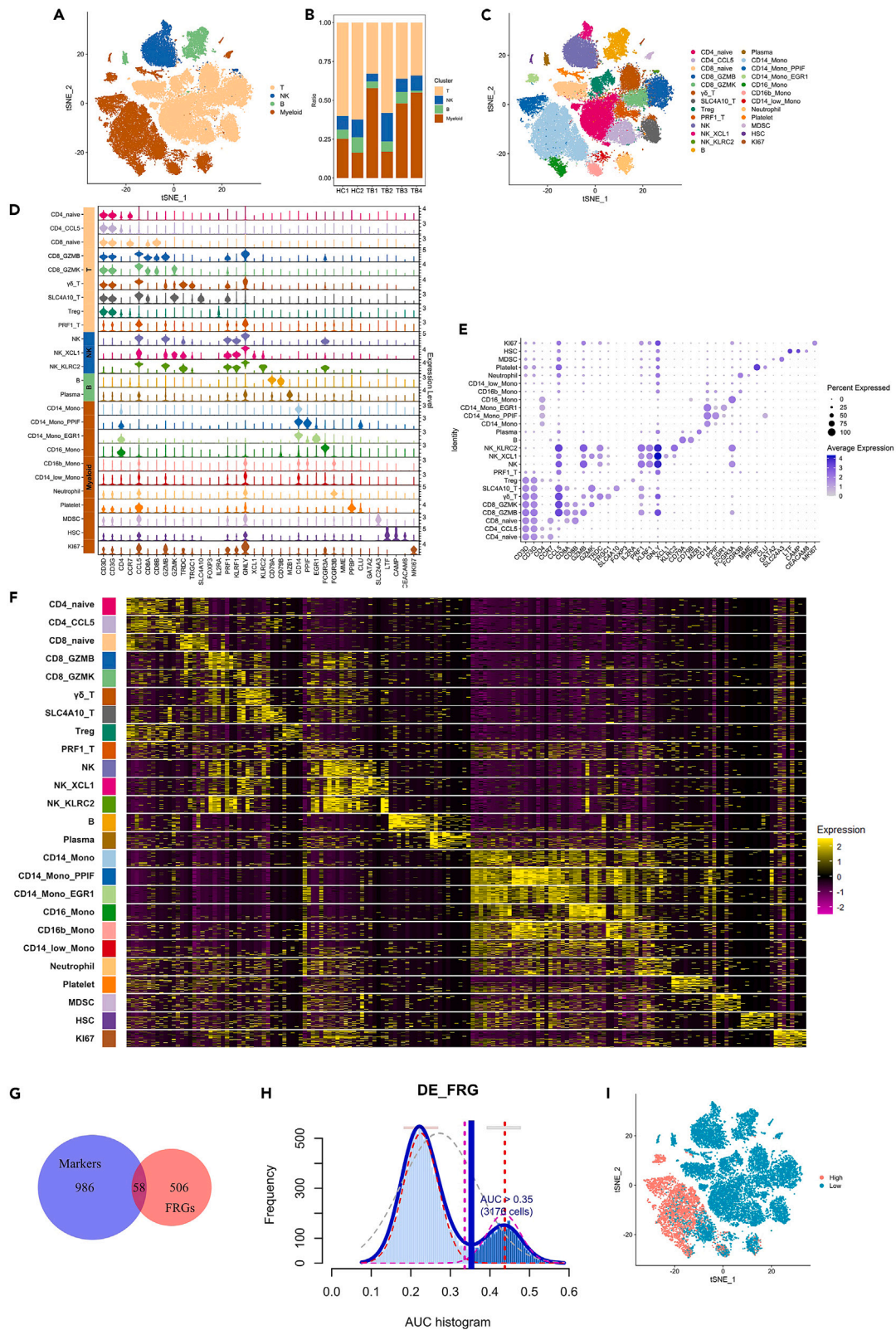


**Figure 1. Single-cell transcriptome of PBMCs from patients with TB and healthy controls**

- (A) Single-cell clusters projected by t-SNE dimension reduction method. Four major cell types were labeled with different colors. Each dot corresponded to a single cell.
- (B) Relative abundance of T, NK, B, and myeloid cells in healthy controls (HC1 and HC2) and patients with TB (TB1, TB2, TB3, and TB4).
- (C) t-SNE projection showing 25 cell clusters labeled with different colors. Legends on the right indicated annotation of cell subtypes.
- (D) Violin plots showing expression levels of selected canonical cell marker genes in the 25 cell clusters. x axis: name of marker genes; y axis: name of cell clusters.
- (E) Dot plots showing expression of selected canonical cell markers in the 25 cell clusters.
- (F) Heatmap showing expression of top 10 cell markers in the 25 cell clusters.
- (G) Venn diagram showing overlapped genes between differentially expressed cell cluster marker genes (Markers) and ferroptosis-related genes (FRGs).
- (H) Area under the curve (AUC) histogram of the 58 ferroptosis-related genes (DE-FRGs). x axis: AUC scores; y axis: number of cells. The threshold was 0.35.
- (I) Expression of 58 ferroptosis-related genes (DE-FRGs) in t-SNE cell clusters. Cells were identified as “high expression” (tangerine color) when AUC score was higher than 0.35, while all other cells were considered “low expression” (cyan color).

Single-cell RNA sequencing (scRNA-seq) is a powerful approach that permits genome-wide gene expression analysis at the single-cell resolution and has been used for discovery of novel cell types and biomarkers that are associated with TB disease.<sup>15–21</sup> A polyfunctional Th17-like T cell subset is found by multimodal T cell profiling to be associated with TB progress.<sup>16</sup> A natural killer (NK) cell subset that can distinguish patients with TB from latent TB infection (LTBI) and healthy controls has been discovered by scRNA-seq.<sup>15</sup> Granzyme-K-expressing CD8 T cells are enriched in pleural fluid of patients with TB and might be used for diagnosis of tuberculous pleurisy.<sup>17</sup> Single-cell profiling identifies granzyme-K-expressing CD8 T cell subsets that probably contribute to protection against TB dissemination.<sup>18</sup> Macrophage subsets in bronchoalveolar lavage fluid (BALF) are associated with TB disease and might be used as biomarker for *Mtb* infection.<sup>20</sup>

Because of association of ferroptosis with TB pathogenesis and dissemination, we postulated that ferroptosis-related genes had the potential to be used as biomarkers for active TB. In this study, expression of ferroptosis-related genes in whole immune cells were analyzed at single-cell resolution by scRNA-seq. By incorporating scRNA-seq data with microarray and bulk RNA-sequencing data, a ferroptosis-related gene signature was identified and evaluated for diagnosis of active TB and association with anti-TB treatment efficacy.

**RESULTS****Single-cell transcriptional atlas of immune cells from patients with active TB**

Single-cell transcriptome was performed on 64,336 cells of PBMCs from patients with TB and age- and sex-matched healthy controls. Cells were clustered based on gene expression profiles by using t-distributed stochastic neighbor embedding (t-SNE) method (Figure 1A). To understand cell types of each cell cluster, gene transcription profiles and cell markers were used to annotate different cell clusters with FindAllMarkers function of Seurat R package. Four major cell types, including T cells, NK cells, B cells, and myeloid cells were identified (Figure 1A). Comparison of relative abundance of the four cell types in patients with TB and healthy controls indicated that patients with TB had lower frequency of T cells and higher ratio of myeloid cells (Figure 1B).

Twenty-five different cell subtypes could be further classified from the t-SNE projection of scRNA-seq data, including CD4<sup>+</sup> T cells (CD4<sub>naive</sub>, CD4<sub>CCL5</sub>), CD8<sup>+</sup> T cells (CD8<sub>naive</sub>, CD8<sub>GZMB</sub>, CD8<sub>GZMK</sub>),  $\gamma\delta$  T cells, SLC4A10<sup>+</sup> T cells (SLC4A10-T), regulatory T cells (Treg), PRF1<sup>+</sup> T cell (PRF1\_T), NK cells (NK, NK<sub>XCL1</sub>, NK<sub>NLRC2</sub>), B cells, plasma cells, CD14<sup>+</sup> monocytes (CD14, CD14<sub>PPIF</sub>, CD14<sub>EGR1</sub>), CD16<sup>+</sup> monocytes (CD16<sub>Mono</sub>), CD16b<sup>+</sup> monocytes (CD16b<sub>Mono</sub>), CD14<sup>low</sup> monocytes (CD14<sub>low</sub><sub>Mono</sub>), neutrophils, platelets, myeloid-derived suppressor cells (MDSCs), hematopoietic stem cells (HSC), and MKI67<sup>+</sup> cells (KI67) (Figures 1C–1F).

**Identification and expression of ferroptosis-related genes in single-cell clusters**

Ferroptosis is a form of regulated cell necrosis triggered by iron overload and lipid peroxidation and contributes to *Mtb* pathogenesis and dissemination.<sup>11,13,14</sup> To further understand the role of ferroptosis in *Mtb* infection, 564 ferroptosis-related genes were obtained from the FerrDb database.<sup>22</sup> Differentially expressed cell markers for cell clusters projected by scRNA-seq data from patients with TB and healthy controls were screened by the FindAllMarkers function of Seurat, and 1,014 cell cluster marker genes were identified. Convergence of the 564 ferroptosis-related genes and 1,014 cell cluster marker genes identified 58 ferroptosis-related genes that were expressed in single-cell clusters of scRNA-seq data (Figure 1G and Table 1).

To know expression profile of the 58 ferroptosis-related genes in single-cell atlas, area under the curve (AUC) was calculated by AUCCell tool to determine enrichment of these gene sets in scRNA-seq data. In general, cells with higher expression levels of ferroptosis-related genes had higher AUC values. When the AUC value was set at 0.35, two distinct cell population was identified and 3,176 cells had an AUC value above the

**Table 1. List of 58 differentially expressed ferroptosis-related genes**

PRKCA, ZEB1, TNFAIP3, PARP8, SLC7A5, JUN, AKR1C3, MEF2C, NCOA3, RB1, FTL, NEAT1, CYBB, FTH1, SAT1, NCF2, BACH1, ACSL1, CTSB, CREB5, FAR1, ALOX5, HIF1A, ATG7, PARP14, CD44, TIMP1, PPARG, ACSL3, LRRFIP1, CD82, DM6B, SLC2A3, VEGFA, ARRDC3, DUSP1, VDR, TGFB1, ACSL4, TLR4, EGR1, FBXW7, HMOX1, BID, HBA1, PTEN, PGRMC1, NCOA4, MAPK14, ABCC1, LCN2, PGD, STMN1, HMGB1, CFL1, RRM2, HELLS, EZH2
--

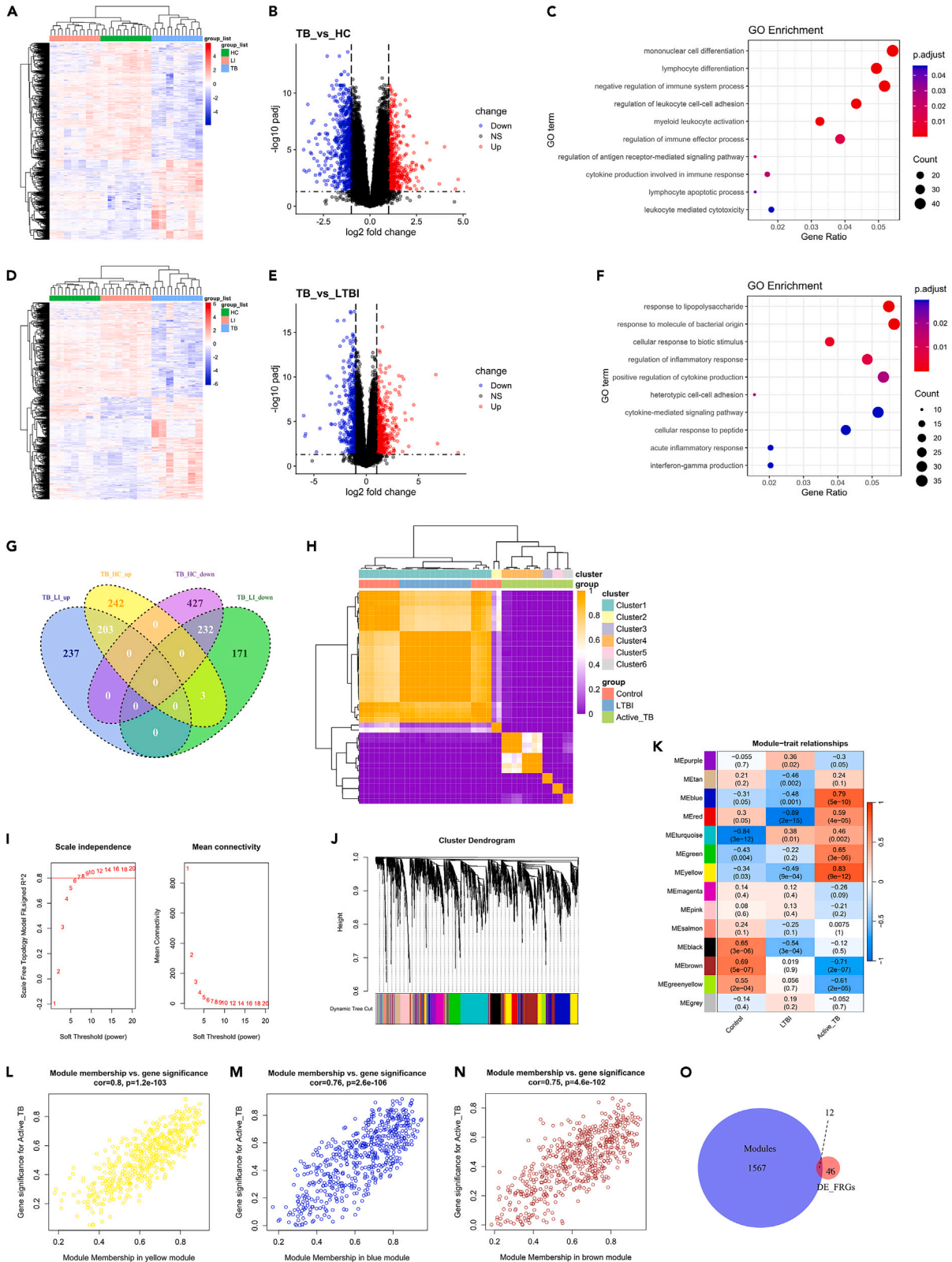


**Figure 2. Analysis of differentially expressed genes (DEGs) in gene expression dataset of GSE62525**

- (A) Heatmap of DEGs among healthy controls (HC), latent TB infection (LI or LTBI), and patients with TB (TB). Red color indicated upregulated genes, and blue color indicated downregulated genes.
- (B) Volcano plots of the DEGs between patients with TB and healthy controls. Blue dots indicated downregulated genes, and red dots indicated upregulated genes.
- (C) GO enrichment analysis of DEGs between patients with TB and healthy controls.
- (D) Heatmap of DEGs among healthy controls, LTBI, and patients with TB.
- (E) Volcano plots of DEGs between patients with TB and LTBI.
- (F) GO enrichment analysis of DEGs between patients with TB and LTBI.
- (G) Venn diagrams of up- and downregulated DEGs between patients with TB and healthy controls (TB\_HC\_up and TB\_HC\_down) and between patients with TB and LTBI (TB\_LI\_up and TB\_LI\_down).
- (H) Consensus clustering analysis of immune-related genes. The colored bars in the upper panel represent different clusters, as indicated in the labels on the right. The colored bars in the lower panel represent different groups of healthy controls, LTBI, and patients with TB, respectively.
- (I) Scale-free fitting index analysis for different soft thresholds ( $R^2 = 0.80$  and power = 8) (left) and mean connectivity for different soft thresholds (right).
- (J) Gene dendrogram obtained by average linkage hierarchical clustering. The colored row underneath the dendrogram indicate modules as determined by the Dynamic Tree Cut.
- (K) Heatmap showing module-trait correlations. Bars on the left column represent modules with different characteristics. Rows represent Pearson correlation coefficient and  $p$  values (within parentheses).
- (L–N) Scatterplots of gene significance for active TB (y axis) vs. module membership (x axis) of the yellow (L), blue (M), and brown (N) modules.
- (O) Venn diagram of genes in the modules (Modules) and the 58 ferroptosis-related genes (DE-FRGs).

threshold (Figure 1H). Further analysis of the 3,176 cells with higher AUC score showed that these gene sets were almost exclusively expressed in cell clusters of myeloid cells (Figure 1I).

**Association of ferroptosis-related genes with active TB**

To investigate genes associated with active TB, gene expression dataset GSE62525 with blood samples of 14 healthy controls, 14 latent TB infection (LTBI), and 14 patients with active TB was retrieved and analyzed. In active TB vs. healthy control groups, 445 genes were upregulated, and 659 genes were downregulated, respectively (Figures 2A and 2B). Gene Ontology (GO) enrichment analysis showed that differentially expressed genes (DEGs) between patients with TB and healthy controls were mainly involved in biological processes (BP) associated with mononuclear cell differentiation, lymphocyte differentiation, negative regulation of immune system process, and regulation of leukocyte cell-cell adhesion (Figure 2C).

There were 843 DEGs, including 440 up- and 403 downregulated genes, in patients with TB vs. LTBI group (Figures 2D and 2E). GO enrichment analysis showed that the DEGs were mainly involved in biological processes (BP) associated with response to lipopolysaccharide, molecule of bacterial origin, cellular response to biotic stimulus, and regulation of inflammatory response (Figure 2F).

Since DEGs among TB, LTBI, and healthy control groups were mainly enriched in pathways involved in immune response, we investigated association of immune-related genes with disease states of TB. Immune-related gene collection was obtained from Immport and InnateDB database.<sup>23,24</sup> Consensus clustering analysis showed that all samples in GSE62525 dataset could be grouped into six clusters (Figure 2H). Clusters 1 and 2 were related to healthy controls and LTBI, whereas clusters 3 to 6 were associated with active TB group (Figure 2H). The result suggested that immune-related genes had the potential to differentiate active TB from latent infection.

Weighted gene coexpression network analysis (WGCNA) has been demonstrated to be an effective method for discovering modules and hub genes related to the clinic-pathological characteristics of diseases.<sup>25</sup> WGCNA was performed to identify key modules related to active TB by using immune-related genes in GSE62525 dataset. The power of  $\beta = 8$  was selected as the soft thresholding value to construct a scale-free network (Figures 2I and 2J). After constructing similar module clustering through dynamic hybrid cutting at a threshold of 0.05, a total of 14 modules were identified (Figure 2K). The Pearson correlation coefficient between clinical characteristics and module eigengenes of each module was calculated. The results showed that yellow (0.83), blue (0.79), and brown (−0.71) modules had the highest correlation to active TB (Figure 2K). Correlation of modules in yellow, blue, and brown with gene significance for active TB was 0.80 ( $p = 1.2e^{-103}$ ), 0.76 ( $p = 2.6e^{-106}$ ), and 0.75 ( $p = 4.6e^{-102}$ ), respectively (Figures 2L–2N). When the module genes were intersected with the 58 ferroptosis-related genes, 12 overlapped genes, including AKR1C3, RB1, CYBB, NCF2, CTSB, CD44, PPARG, CD82, VDR, ACSL4, TLR4, and BID, were found to be associated with active TB and were used for further analysis (Figure 2O).

**Trajectory analysis of ferroptosis-related genes**

Correlation analysis was performed among the 12 ferroptosis-related genes (Figure 3A). The positive correlation between CYBB and NCF2 was statistically significant ( $r = 0.63$ ,  $p < 0.001$ ). CTSB was positively correlated with CYBB ( $r = 0.60$ ,  $p < 0.001$ ) and NCF2 ( $r = 0.51$ ,  $p < 0.001$ ). TLR4 presented a significantly positive correlation with CYBB ( $r = 0.52$ ,  $p < 0.001$ ) and NCF2 ( $r = 0.46$ ,  $p < 0.001$ ). AKR1C3 was negatively correlated with the other 11 genes (Figure 3A).

Expression of the 12 ferroptosis-related genes in single-cell clusters was examined. AKR1C3 was dominantly expressed in NK cells, whereas CD44 and RB1 were expressed in most cell clusters (Figure 3B). The other nine genes were predominantly expressed in myeloid cells (Figure 3B).

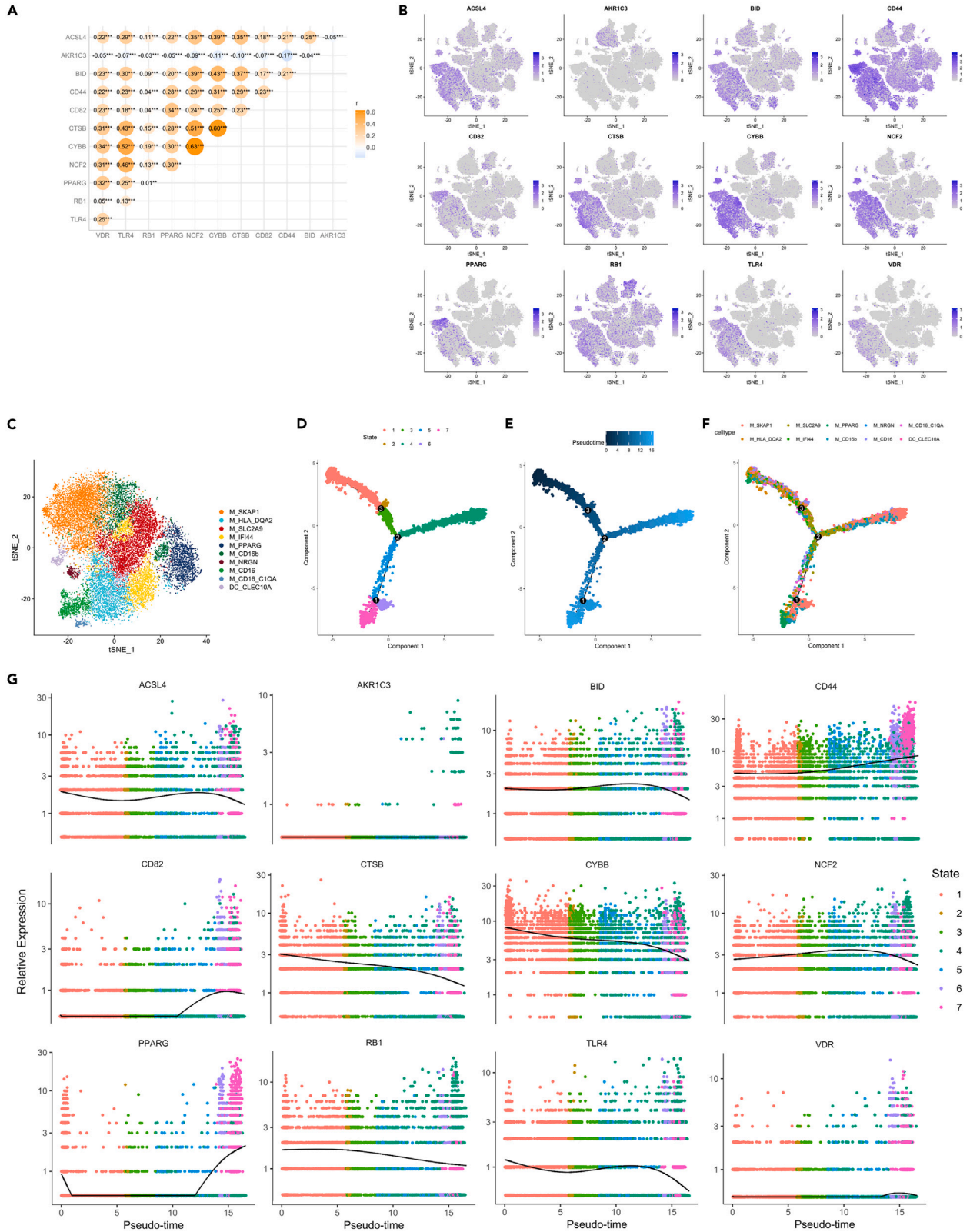


**Figure 3. Expression of the 12 ferroptosis-related genes and pseudotime analysis of myeloid cells**

- (A) Correlation analysis of the 12 ferroptosis-related genes. Gene names were shown in x- and y axis. The numbers in the figure indicate correlation coefficient “r”, and asterisk indicates p values. \*\*\* $p < 0.001$ ; \*\* $p < 0.01$ .
- (B) Expression patterns of the 12 ferroptosis-related genes in t-SNE cell clusters of scRNA-seq data. The expression levels of genes were indicated in the bar on the right panel of each plot.
- (C) Cell clusters of myeloid cells were projected by t-SNE method. Each dot on the plot represents one cell. The legends on the right panel indicate annotation of different myeloid cell clusters.
- (D and E) Cell trajectory differentiation analysis of myeloid cells. Seven differentiation states (D) and pseudotime (E) were analyzed.
- (F) Location of the 10 myeloid cell clusters along the trajectory differentiation pseudotime. The 10 myeloid cell clusters were labeled with different colors, as shown in the top panel.
- (G) Relative expression profiles of the 12 ferroptosis-related genes during the differentiation pseudotime trajectory. x axis shows pseudotime, and y axis indicates expression levels of genes. Different colors indicate different differentiation states.

To further analyze myeloid cells, 18,793 cells annotated as myeloid cells were extracted from scRNA-seq data, and 10 cell clusters were identified by t-SNE projection (Figure 3C). Myeloid cell clusters were annotated based on different immune cell markers and included CD14<sup>+</sup> monocytes (M\_SKAP1, M\_HLA\_DQA2, M\_SLC2A9, M\_IFI44, M\_PPARG, M\_CD16b, and M\_NRGN), CD16<sup>+</sup> monocytes (M\_CD16 and M\_CD16\_C1QA), and dendritic cells (DC) (DC\_CLEC10A) (Figure 3C).

Simulation analysis on the cell trajectory differentiation of all myeloid cells was carried out. Seven differentiated cell states were observed and labeled by distinct colors (Figure 3D). As shown in label on the top of Figure 3E, the darker to light blue manifested different cell differentiation states over time. M\_HLA\_DQA2 and M\_IFI44 cell clusters were mainly found at the beginning of differentiation and might be differentiated into M\_SKAP1 and M\_PPARG cells (Figure 3F). The expression of 12 ferroptosis-related genes changed with different differentiation states (Figure 3G). Along the trajectory, the expression levels of CD44, CD82, and PPARG were gradually increased during the transition. The opposite trends could be seen in CTSB, CYBB, RB1, and TLR4 (Figure 3G).

**Screening of ferroptosis-related genes with diagnostic value by machine learning algorithms**

Three machine learning algorithms, LASSO (Least Absolute Shrinkage and Selection Operator), All Subset Regression, and Stepwise Regression, were utilized for screening the 12 ferroptosis-related genes with diagnostic potential. LASSO analysis found that five genes (ACSL4, CTSB, PPARG, TLR4, and VDR) were associated with active TB (Figures 4A and 4B). Stepwise Regression identified six genes (ACSL4, CD82, CTSB, CYBB, PPARG, and TLR4) that were associated with active TB, while All Subset Regression found four genes (ACSL4, CTSB, CYBB, and TLR4) (Figure 4C). Convergence of the three machine learning algorithms identified three genes (ACSL4, CTSB, and TLR4) that were designated as ferroptosis-related gene signature (Figure 4D).

**Evaluation of ferroptosis-related gene signature for diagnosis of active TB**

Ferroptosis-related gene signature containing ACSL4, CTSB, and TLR4 genes were evaluated for diagnosis of TB. Four datasets, GSE62525, GSE107991, GSE107994, and GSE39941, which contained gene expression data from blood samples of healthy controls, LTBI, patients with TB, and patients with other diseases, were used as test dataset (GSE62525) and validation datasets (GSE107991, GSE107994, and GSE39941), respectively. The expression levels of ACSL4, CTSB, and TLR4 genes were significantly higher in patients with TB than in LTBI and/or healthy controls in all four datasets (Figures 4E, 4G, 4I, and 4K). To determine the diagnostic potential of the gene signature, receiver operating characteristic (ROC) analysis was performed and the area under the ROC curve (AUC) was calculated. The AUCs for the gene signature were 1.000, 0.906, and 0.974 for differentiating TB from healthy controls (Figures 4F, 4H, and 4J). For differentiating TB from LTBI, the AUCs were 1.000, 0.866, 0.912, and 0.786 in the four datasets, respectively (Figures 4F, 4H, 4J, and 4L). The AUC was 0.626 for differentiating TB from other diseases.

The results demonstrated that 3-gene-ferroptosis-related signature was a promising biomarker to distinguish active TB from LTBI.

**Association of ferroptosis-related gene signature with TB treatment efficacy**

To assess the prognostic value of the ferroptosis-related gene signature, GSE89403 gene expression dataset with 50 healthy controls, 142 patients with cured TB, and 14 patients with failed TB treatment were examined. Failed TB treatment was diagnosed when *Mtb* culture was positive after 6 months of standard anti-TB treatment, whereas cured TB was defined as disappearance of clinical manifestation and negative *Mtb* detection after six months of treatment. The samples were divided into three groups: healthy controls, cures, and failures, while the cures were split into four groups according to the time of bacteriological conversion. Expression of the signature genes was highest in the failed treatment group at the time of diagnosis (Figures 5A, 5C, and 5E). During the course of anti-TB treatment, expression of the signature genes decreased rapidly in the fast bacteriological conversion groups of cured patients with TB, while much less change of expression was observed in the group of failed patients (Figures 5B, 5D, and 5F).

GSE157657 gene set, with 38 healthy controls and 45 patients with active TB, was used to validate the prognostic value of the ferroptosis-related gene signature as well. Patients with TB were further divided into short anti-TB treatment (short-ATT) group with 15 patients and long anti-TB treatment group (long-ATT) with 30 patients. Patients with drug-sensitive TB who were cured with less than 200 days to anti-TB treatment were considered as short-ATT, whereas those required more than 200 days of treatment were classified into long-ATT group. Expression levels of the three ferroptosis-related signature genes were highest at the time of diagnosis in the long-ATT group (Figures 6A, 6C, and 6E).

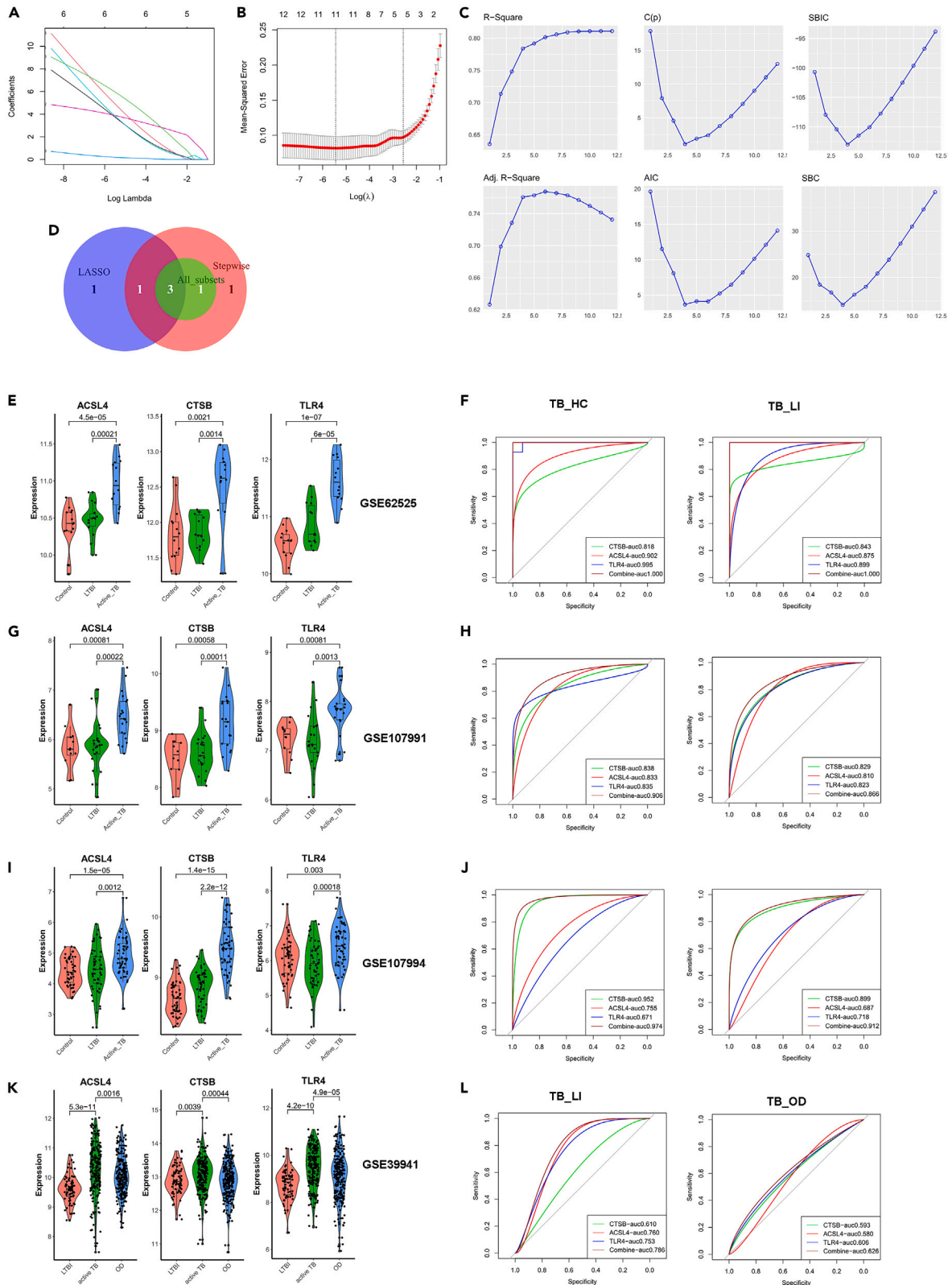


**Figure 4. Identification of ferroptosis-related gene signature by machine learning algorithms and evaluation of diagnostic potential for TB**

(A and B) Ferroptosis-related gene signature was identified by machine learning algorithm LASSO. The variation characteristics of the coefficient of variables (A) and the optimum value of parameter in the LASSO regression model by cross-validation method ( $\lambda_{\text{mda.1se}} = 0.0485$ ) (B) are shown.

(C) Identification of hub genes by All Subset Regression. There were 4,095 possible models. The line graphs show values of R-square, C(p) (Mallows Cp), SBIC (Sawa's Batesian Information Criteria), adjust R-square, AIC (Akaike Information Criteria), and SBC (Schwarz Bayesian Criteria) of the best subsets (y axis) associated with number of genes (x axis).

(D) Venn diagram of hub genes identified by LASSO, All Subset Regression, and Stepwise Regression.

(E, G, I, and K) Violin plots showing normalized gene expression levels and inter-quartile range (IQR) of the hub genes in healthy controls (Control), latent TB infection (LTBI), and patients with active TB (Active\_TB) in the gene expression datasets of GSE62525 (E), GSE10791 (G), GSE107994 (I), and GSE39941 (K). Each dot represents one sample.

(F, H, J, and L) ROC analysis of the ferroptosis-related gene signature for differentiating active TB from healthy controls (TB\_HC), active TB from LTBI (TB\_LI), and active TB from other diseases (TB\_OD) in the gene expression datasets GSE62525 (F), GSE107991 (H), GSE107994 (J), and GSE39941 (L). The area under the ROC curve for ACSL4, CTSB, TLR4, and combined gene signature is shown on the lower right corner.

During the course of anti-TB treatment, expression of the signature genes decreased rapidly in the short-ATT group of patients with TB, while change of expression was slower in the long-ATT group (Figures 6B, 6D, and 6F).

These results indicated the ferroptosis-related gene signature was associated with anti-TB treatment efficacy.

**DISCUSSION**

Unlike bulk RNA-sequencing and microarray transcriptional analysis, scRNA-seq is a high-throughput technology that detects transcriptome in each single cell.<sup>26,27</sup> Therefore, it reveals composition of different cell types in tissues and organs and allows visualization of RNA expression levels in single cells.<sup>26,27</sup> In this study, we identified three ferroptosis-related genes that were associated with TB disease by incorporating scRNA-seq data with microarray and bulk RNA-sequencing data. Comparison of mRNA expression levels in different scRNA-seq cell clusters demonstrated that the three ferroptosis-related genes were predominantly expressed in myeloid cells.

Diagnosis of TB remains a challenge when microbiological tests are negative. Host blood transcriptomics have been used extensively to screen biomarkers for diagnosis of TB and prediction of progression to TB disease.<sup>28–30</sup> Selected blood transcriptional signatures for diagnosis of active TB are evaluated in a recent study, and four signatures achieve sensitivities between 83.3% and 90.7% when 70% specificity is used as a threshold.<sup>3</sup>

Patients with TB have elevated frequency of monocytes and increased monocyte-to-lymphocyte ratio in the blood.<sup>19,31</sup> Classical CD14<sup>+</sup>CD16<sup>-</sup> and intermediate CD14<sup>+</sup>CD16<sup>+</sup> monocytes are responsible for the increased monocyte-to-lymphocyte ratio.<sup>31</sup> In consistent with these results, our scRNA-seq data showed that three out of four patients with TB had increased abundance of myeloid cells in the peripheral blood. Some myeloid cell clusters were probably associated with TB.

A bioinformatics analysis of blood microarray transcriptional datasets identifies three ferroptosis-related genes, CHMP5, SAT1, and ZFP36, as potential diagnostic biomarkers for TB.<sup>32</sup> Nine ferroptosis-related hub genes, MAPK14, EGLN2, IDO1, USP11, SCD, CBS, PARP8, PARP16, and CDC25A, were identified by analyzing data from Gene Expression Omnibus (GEO).<sup>33</sup> These genes correlate with TB disease and are potential biomarkers for differentiating latent from active TB in children.<sup>33</sup> Ferroptosis-related gene SOCS1 expression is significantly upregulated in patients with TB and decreases following standard anti-TB treatment.<sup>34</sup>

The three ferroptosis-related gene signatures identified in this study included ACSL4, CTSB, and TLR4 genes. ACSL4 is an isoenzyme of long-chain acyl-CoA synthase (ACSL) that catalyzes free fatty acids with 10–22 carbons to fatty acyl-CoAs, a first step in the metabolism of fatty acids.<sup>35</sup> ACSL4 promotes ferroptosis in the absence of GPX4 by synthesizing arachidonoyl-CoA (AA-CoA) that converts into lipid peroxides (LPOs) on cellular membranes.<sup>35–37</sup> ACSL4 is associated with resistance to *Mtb* infection in highly exposed contacts.<sup>38</sup> A 10 lipid-related gene signature containing ACSL4 had significant alterations during the course of anti-TB treatment.<sup>39</sup> ACSL4 is associated with anti-TB drug-induced hepatocyte damage, which is reversed by specific ferroptosis inhibitor.<sup>40</sup>

Cathepsin B (CTSB) is a widely expressed lysosomal cysteine protease and involves in intracellular proteolysis and many physiological and pathological processes.<sup>41</sup> CTSB is a major cause of ferroptosis independent of the GSH/GPX4 axis, probably by cleavage of histone H3.<sup>42</sup> Nuclear accumulation of CTSB released from the lysosome causes DNA damage and ferroptosis.<sup>43</sup> CTSB is elevated in plasma of patients with active TB and also in the lungs of *Mtb*-infected mice.<sup>44</sup> Lysosomal release of CTSB is probably required for NLRP3-inflammasome activation of macrophages by *Mtb*.<sup>44</sup>

Toll-like receptors (TLRs) are pattern recognition receptors involving in innate immunity.<sup>45</sup> Toll-like receptor 4 (TLR4) expresses mainly in immune cells and functions through MyD88-dependent and MyD88-independent signaling pathways.<sup>45</sup> TLR4/IKK $\beta$  pathway regulates ceramide synthetase 6 (CerS6) synthesis to induce mitochondrial oxidative stress and promotes ferroptosis of human normal liver cells.<sup>46</sup> TLR4 mutant C3H/HeJ mice infected with *Mtb* have more severe disease and higher bacterial burden in the lungs.<sup>47,48</sup>

A number of cytokines, such as IFN- $\gamma$ -induced protein 10 (IP-10/CXCL10), were promising biomarkers for diagnosis of TB infection.<sup>49,50</sup> However, IP-10 was not listed as ferroptosis-related molecule and was not included in the study. Metagenomic sequencing of microbes reveals that gut and lung microbiota are associated with TB susceptibility, disease progression, and treatment.<sup>51–56</sup> Simultaneous host transcriptome and gut-lung microbiome analysis might be useful for TB diagnosis and therapeutics.

In conclusion, an immune cell atlas of patients with active TB and healthy controls were established by scRNA-seq. Through integrated analysis scRNA-seq data with microarray and bulk-RNA sequencing data, a three gene ferroptosis-related signature for TB was identified. The ferroptosis-related gene signature was associated with TB treatment efficacy and was a promising biomarker to differentiate active TB from latent TB infection.

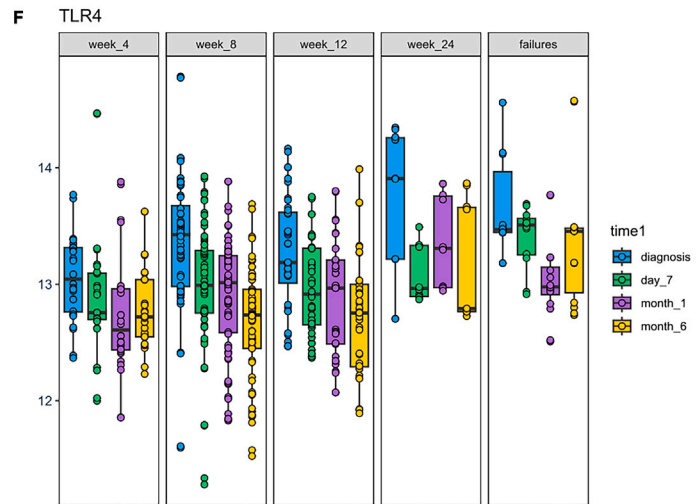
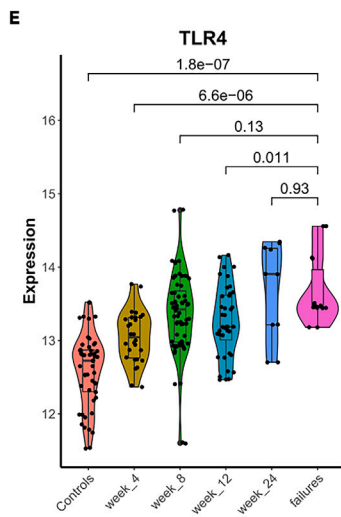
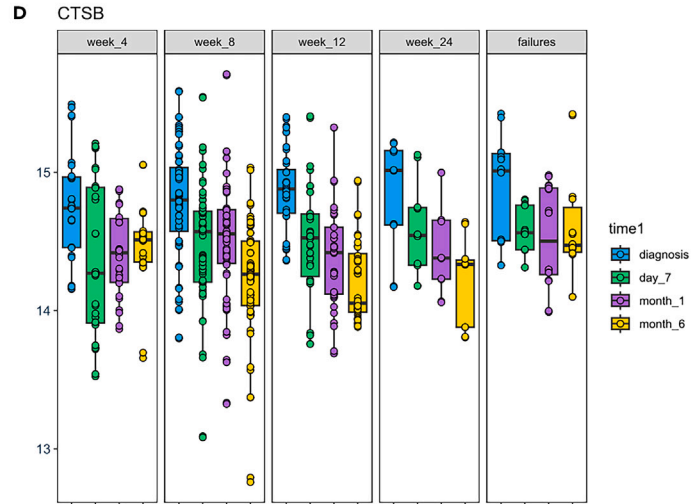
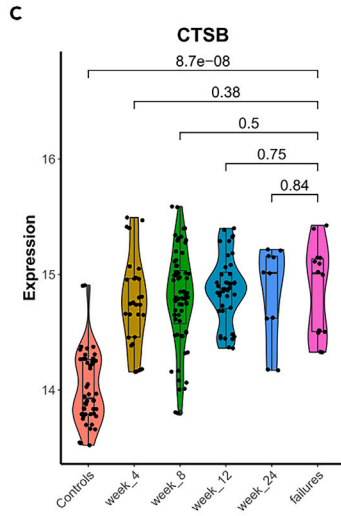
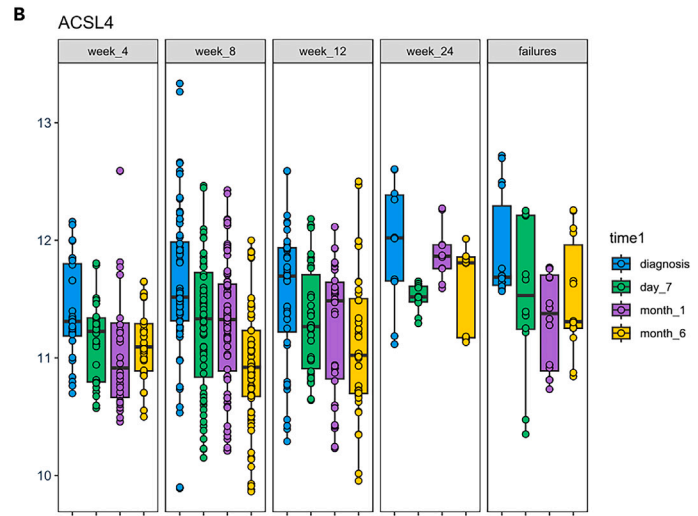
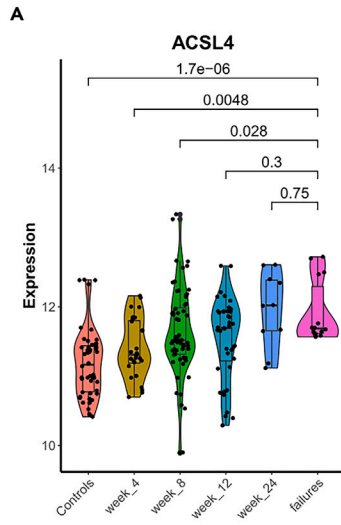


**Figure 5. Association of ferroptosis-related gene signature with anti-TB treatment efficacy in GSE89403 gene set**

(A) Scatter violin plots showing expression levels of ACSL4 gene in healthy controls (Controls) and different groups of patients with TB. Patients with TB were divided into five groups according to the time of bacteriological conversion: negative conversion of *Mtb* results at 4 weeks (week\_4), 8 weeks (week\_8), 12 weeks (week\_12), and 24 weeks (week\_24) of anti-TB treatment or failed treatment (failures) (x axis). y axis: expression levels of gene. Each dot represents one sample of either patients or controls. p value is shown on the top of plots.

(B) Scatterplots showing expression levels of ACSL4 gene in different groups of patients with TB as indicated in upper panel. The bar and dots in different color show expression levels of ACSL4 gene at the time of diagnosis (diagnosis), and 7 days (day\_7), 1 month (month\_1), and 6 months (month\_6) after anti-TB treatment (right panel).

(C) Scatter violin plots showing expression levels of CTSB gene in healthy controls and different groups of TB patients.

(D) Scatterplots showing expression levels of CTSB gene at different time points of anti-TB treatment.

(E) Scatter violin plots showing expression levels of TLR4 gene in healthy controls and different groups of TB patients.

(F) Scatterplots showing expression levels of TLR4 gene at different time points of anti-TB treatment.

**Limitations of the study**

Integrated analysis of scRNA-sequencing with microarray and bulk RNA-sequencing data investigated RNA expression of genes only, and their protein expression levels were not determined. scRNA-seq was performed on patients with active TB and healthy controls, not on LTBI.

**STAR★METHODS**

Detailed methods are provided in the online version of this paper and include the following:

- [KEY RESOURCES TABLE](#)
- [RESOURCE AVAILABILITY](#)
  - Lead contact
  - Materials availability
  - Data and code availability
- [EXPERIMENTAL MODEL AND STUDY PARTICIPANT DETAILS](#)
- [METHOD DETAILS](#)
  - Purification of peripheral blood mononuclear cells (PBMCs)
  - Single-cell library construction
  - Single-cell transcriptome data analysis
  - Principal component analysis and annotation of cell clusters
  - Ferroptosis-related gene scoring
  - Pseudotime analysis
  - Dataset collection and processing
  - Identification of differentially expressed genes (DEGs) and gene ontology enrichment analysis
  - Consensus clustering analysis
  - Weighted gene co-expression network analysis
  - Screening of ferroptosis-related genes with diagnostic value by machine learning algorithms
- [QUANTIFICATION AND STATISTICAL ANALYSIS](#)

**ACKNOWLEDGMENTS**

This work was supported by grant from National Natural Science Foundation of China, China (grant numbers: 82072233 and 82270020). We thank Dr. Chenhai Wang for his valuable help in data analysis and statistics.

**AUTHOR CONTRIBUTIONS**

Conceptualization: X.C. and B.Y.; data curation: B.Y. and F.Z.; formal analysis: B.Y.; funding acquisition: X.C. and J.J.; investigation: B.Y., F.Z., Z.L., X.W., X.D., Z.C., L.Y., J.J., and R.W.; resources: Z.L. and X.W.; writing—original draft: B.Y.; writing—review & editing: X.C. and B.Y.

**DECLARATION OF INTERESTS**

The authors declare no competing interests.

Received: December 18, 2023

Revised: March 4, 2024

Accepted: June 1, 2024

Published: June 4, 2024

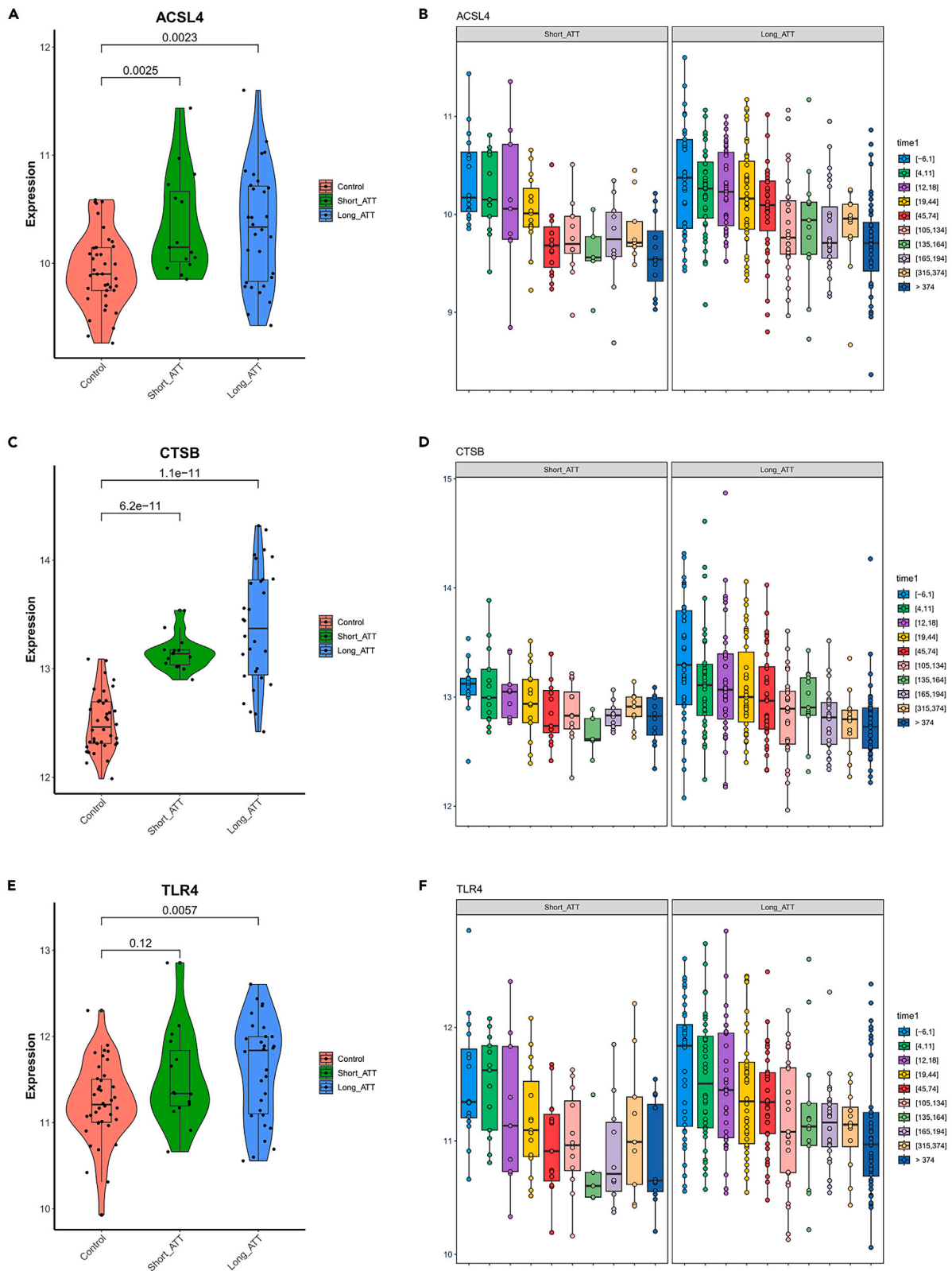


**Figure 6. Association of ferroptosis-related gene signature with anti-TB treatment efficacy in GSE157657 gene set**

- (A) Scatter violin plots showing expression levels of ACSL4 gene in healthy controls (Control), short anti-TB treatment group (Short-ATT), and long anti-TB treatment group (Long-ATT) of patients with TB. Each dot represents one sample of either patients or controls. *p* value is shown on the top of plots.
- (B) Scatterplots showing expression levels of ACSL4 gene at different time points of short-ATT and long-ATT groups of patients with TB. The time points of anti-TB treatment were shown on the right with different colors (time1).
- (C) Scatter violin plots showing expression levels of CTSB gene in healthy controls and short and long anti-TB treatment groups of patients with TB.
- (D) Scatterplots showing expression levels of CTSB gene at different time points of anti-TB treatment.
- (E) Scatter violin plots showing expression levels of TLR4 gene in healthy controls and short and long anti-TB treatment groups of patients with TB.
- (F) Scatterplots showing expression levels of TLR4 gene at different time points of anti-TB treatment.

**REFERENCES**

- WHO (2023). Global Tuberculosis Report 2023. <https://www.who.int/publications/item/9789240083851>.
- WHO Guidelines Approved by the Guidelines Review Committee (2022). In WHO consolidated guidelines on tuberculosis: Module 3: Diagnosis – Tests for tuberculosis infection (World Health Organization@ World Health Organization, 2022).
- Turner, C.T., Gupta, R.K., Tsaliki, E., Roe, J.K., Mondal, P., Nyawo, G.R., Palmer, Z., Miller, R.F., Reeve, B.W., Theron, G., and Noursadeghi, M. (2020). Blood transcriptional biomarkers for active pulmonary tuberculosis in a high-burden setting: a prospective, observational, diagnostic accuracy study. *Lancet Respir. Med.* 8, 407–419. [https://doi.org/10.1016/s2213-2600\(19\)30469-2](https://doi.org/10.1016/s2213-2600(19)30469-2).
- Chandra, P., Grigsby, S.J., and Philips, J.A. (2022). Immune evasion and provocation by *Mycobacterium tuberculosis*. *Nat. Rev. Microbiol.* 20, 750–766. <https://doi.org/10.1038/s41579-022-00763-4>.
- Chai, Q., Wang, L., Liu, C.H., and Ge, B. (2020). New insights into the evasion of host innate immunity by *Mycobacterium tuberculosis*. *Cell. Mol. Immunol.* 17, 901–913. <https://doi.org/10.1038/s41423-020-0502-z>.
- Liu, C.H., Liu, H., and Ge, B. (2017). Innate immunity in tuberculosis: host defense vs pathogen evasion. *Cell. Mol. Immunol.* 14, 963–975. <https://doi.org/10.1038/cmi.2017.88>.
- Nisa, A., Kipper, F.C., Panigrahy, D., Tiwari, S., Kupz, A., and Subbian, S. (2022). Different modalities of host cell death and their impact on *Mycobacterium tuberculosis* infection. *Am. J. Physiol. Cell Physiol.* 323, C1444–C1474. <https://doi.org/10.1152/ajpcell.00246.2022>.
- Jorgensen, I., Rayamajhi, M., and Miao, E.A. (2017). Programmed cell death as a defence against infection. *Nat. Rev. Immunol.* 17, 151–164. <https://doi.org/10.1038/nri.2016.147>.
- Stockwell, B.R., Friedmann Angeli, J.P., Bayir, H., Bush, A.I., Conrad, M., Dixon, S.J., Fulda, S., Gascón, S., Hatzios, S.K., Kagan, V.E., et al. (2017). Ferroptosis: A Regulated Cell Death Nexus Linking Metabolism, Redox Biology, and Disease. *Cell* 171, 273–285. <https://doi.org/10.1016/j.cell.2017.09.021>.
- Dixon, S.J., Lemberg, K.M., Lamprecht, M.R., Skouta, R., Zaitsev, E.M., Gleason, C.E., Patel, D.N., Bauer, A.J., Cantley, A.M., Yang, W.S., et al. (2012). Ferroptosis: an iron-dependent form of nonapoptotic cell death. *Cell* 149, 1060–1072. <https://doi.org/10.1016/j.cell.2012.03.042>.
- Amaral, E.P., Costa, D.L., Namasivayam, S., Riteau, N., Kamenyeva, O., Mittereder, L., Mayer-Barber, K.D., Andrade, B.B., and Sher, A. (2019). A major role for ferroptosis in *Mycobacterium tuberculosis*-induced cell death and tissue necrosis. *J. Exp. Med.* 216, 556–570. <https://doi.org/10.1084/jem.20181776>.
- Yang, W.S., SriRamaratnam, R., Welsch, M.E., Shimada, K., Skouta, R., Viswanathan, V.S., Cheah, J.H., Clemons, P.A., Shamji, A.F., Clish, C.B., et al. (2014). Regulation of ferroptotic cancer cell death by GPX4. *Cell* 156, 317–331. <https://doi.org/10.1016/j.cell.2013.12.010>.
- Amaral, E.P., Foreman, T.W., Namasivayam, S., Hilligan, K.L., Kauffman, K.D., Barbosa Bomfim, C.C., Costa, D.L., Barreto-Duarte, B., Gurgel-Rocha, C., Santana, M.F., et al. (2022). GPX4 regulates cellular necrosis and host resistance in *Mycobacterium tuberculosis* infection. *J. Exp. Med.* 219, e20220504. <https://doi.org/10.1084/jem.20220504>.
- Qiang, L., Zhang, Y., Lei, Z., Lu, Z., Tan, S., Ge, P., Chai, Q., Zhao, M., Zhang, X., Li, B., et al. (2023). A mycobacterial effector promotes ferroptosis-dependent pathogenicity and dissemination. *Nat. Commun.* 14, 1430. <https://doi.org/10.1038/s41467-023-37148-x>.
- Cai, Y., Dai, Y., Wang, Y., Yang, Q., Guo, J., Wei, C., Chen, W., Huang, H., Zhu, J., Zhang, C., et al. (2020). Single-cell transcriptomics of blood reveals a natural killer cell subset depletion in tuberculosis. *EBioMedicine* 53, 102686. <https://doi.org/10.1016/j.ebiom.2020.102686>.
- Nathan, A., Beynor, J.I., Baglaenko, Y., Suliman, S., Ishigaki, K., Asgari, S., Huang, C.C., Luo, Y., Zhang, Z., Lopez, K., et al. (2021). Multimodally profiling memory T cells from a tuberculosis cohort identifies cell state associations with demographics, environment and disease. *Nat. Immunol.* 22, 781–793. <https://doi.org/10.1038/s41590-021-00933-1>.
- Cai, Y., Wang, Y., Shi, C., Dai, Y., Li, F., Xu, Y., Zhang, P., Kong, F., Deng, G., Wen, Z., et al. (2022). Single-cell immune profiling reveals functional diversity of T cells in tuberculosis pleural effusion. *J. Exp. Med.* 219, e20211777. <https://doi.org/10.1084/jem.20211777>.
- Jiang, J., Cao, Z., Xiao, L., Su, J., Wang, J., Liang, J., Yang, B., Liu, Y., Zhai, F., Wang, R., and Cheng, X. (2023). Single-cell profiling identifies T cell subsets associated with control of tuberculosis dissemination. *Clin. Immunol.* 248, 109266. <https://doi.org/10.1016/j.clim.2023.109266>.
- Wang, Y., Sun, Q., Zhang, Y., Li, X., Liang, Q., Guo, R., Zhang, L., Han, X., Wang, J., Shao, L., et al. (2023). Systemic immune dysregulation in severe tuberculosis patients revealed by a single-cell transcriptome atlas. *J. Infect.* 86, 421–438. <https://doi.org/10.1016/j.jinf.2023.03.020>.
- Wang, Q., Qi, F., Ye, T., Li, J., Xu, G., He, X., Deng, G., Zhang, P., Liao, M., Qiao, K., and Zhang, Z. (2023). The interaction of macrophages and CD8 T cells in bronchoalveolar lavage fluid is associated with latent tuberculosis infection. *Emerg. Microbes Infect.* 12, 2239940. <https://doi.org/10.1080/22221751.2023.2239940>.
- Wang, L., Ma, H., Wen, Z., Niu, L., Chen, X., Liu, H., Zhang, S., Xu, J., Zhu, Y., Li, H., et al. (2023). Single-cell RNA-sequencing reveals heterogeneity and intercellular crosstalk in human tuberculosis lung. *J. Infect.* 87, 373–384. <https://doi.org/10.1016/j.jinf.2023.09.004>.
- Zhou, N., Yuan, X., Du, Q., Zhang, Z., Shi, X., Bao, J., Ning, Y., and Peng, L. (2023). FerrDb V2: update of the manually curated database of ferroptosis regulators and ferroptosis-disease associations. *Nucleic Acids Res.* 51, D571–D582. <https://doi.org/10.1093/nar/gkac935>.
- Breuer, K., Foroushani, A.K., Laird, M.R., Chen, C., Sribnaia, A., Lo, R., Winsor, G.L., Hancock, R.E.W., Brinkman, F.S.L., and Lynn, D.J. (2013). InnateDB: systems biology of innate immunity and beyond—recent updates and continuing curation. *Nucleic Acids Res.* 41, D1228–D1233. <https://doi.org/10.1093/nar/gks1147>.
- Bhattacharya, S., Dunn, P., Thomas, C.G., Smith, B., Schaefer, H., Chen, J., Hu, Z., Zalocusky, K.A., Shankar, R.D., Shen-Orr, S.S., et al. (2018). ImmPort, toward repurposing of open access immunological assay data for translational and clinical research. *Sci. Data* 5, 180015. <https://doi.org/10.1038/sdata.2018.15>.
- Liu, Z., Zhu, Z., Huang, Y., Nong, S., Jiang, M., Yi, S., Xie, D., and Hu, H. (2023). Identification of gene modules and hub genes associated with *Colletotrichum siamense* infection in mango using weighted gene co-expression network analysis. *BMC Genom.* 24, 710. <https://doi.org/10.1186/s12864-023-09811-6>.
- Jovic, D., Liang, X., Zeng, H., Lin, L., Xu, F., and Luo, Y. (2022). Single-cell RNA sequencing technologies and applications: A brief overview. *Clin. Transl. Med.* 12, e694. <https://doi.org/10.1002/ctm2.694>.
- Aldridge, S., and Teichmann, S.A. (2020). Single cell transcriptomics comes of age. *Nat. Commun.* 11, 4307. <https://doi.org/10.1038/s41467-020-18158-5>.
- Mulenga, H., Zauchenberger, C.Z., Bunyasi, E.W., Mbandi, S.K., Mendelsohn, S.C., Kagina, B., Penn-Nicholson, A., Scriba, T.J., and Hatherill, M. (2020). Performance of diagnostic and predictive host blood transcriptomic signatures for Tuberculosis disease: A systematic review and meta-analysis. *PLoS One* 15, e0237574. <https://doi.org/10.1371/journal.pone.0237574>.
- Kaforou, M., Broderick, C., Vito, O., Levin, M., Scriba, T.J., and Seddon, J.A. (2022). Transcriptomics for child and adolescent

- tuberculosis. *Immunol. Rev.* 309, 97–122. <https://doi.org/10.1111/imr.13116>.
30. Burel, J.G., Babor, M., Pomaznoy, M., Lindestam Arlehamn, C.S., Khan, N., Sette, A., and Peters, B. (2019). Host Transcriptomics as a Tool to Identify Diagnostic and Mechanistic Immune Signatures of Tuberculosis. *Front. Immunol.* 10, 221. <https://doi.org/10.3389/fimmu.2019.00221>.
  31. Hillman, H., Khan, N., Singhanian, A., Dubelko, P., Soldevila, F., Tippalagama, R., DeSilva, A.D., Gunasena, B., Perera, J., Scriba, T.J., et al. (2022). Single-cell profiling reveals distinct subsets of CD14<sup>+</sup> monocytes drive blood immune signatures of active tuberculosis. *Front. Immunol.* 13, 1087010. <https://doi.org/10.3389/fimmu.2022.1087010>.
  32. Wufuer, D., Li, Y., Aierken, H., and Zheng, J. (2023). Bioinformatics-led discovery of ferroptosis-associated diagnostic biomarkers and molecule subtypes for tuberculosis patients. *Eur. J. Med. Res.* 28, 445. <https://doi.org/10.1186/s40001-023-01371-5>.
  33. Chen, L., Hua, J., Dai, X., and He, X. (2023). Assessment of ferroptosis-associated gene signatures as potential biomarkers for differentiating latent from active tuberculosis in children. *Microb. Genom.* 9, mgen000997. <https://doi.org/10.1099/mgen.0.000997>.
  34. Liang, T., Chen, J., Xu, G., Zhang, Z., Xue, J., Zeng, H., Jiang, J., Chen, T., Qin, Z., Li, H., et al. (2022). Ferroptosis-related gene SOCS1, a marker for tuberculosis diagnosis and treatment, involves in macrophage polarization and facilitates bone destruction in tuberculosis. *Tuberculosis* 132, 102140. <https://doi.org/10.1016/j.tube.2021.102140>.
  35. Ding, K., Liu, C., Li, L., Yang, M., Jiang, N., Luo, S., and Sun, L. (2023). Acyl-CoA synthase ACSL4: an essential target in ferroptosis and fatty acid metabolism. *Chin. Med. J.* 136, 2521–2537. <https://doi.org/10.1097/cm9.0000000000002533>.
  36. Gan, B. (2022). ACSL4, PUFA, and ferroptosis: new arsenal in anti-tumor immunity. *Signal Transduct. Targeted Ther.* 7, 128. <https://doi.org/10.1038/s41392-022-01004-z>.
  37. Liao, P., Wang, W., Wang, W., Kryczek, I., Li, X., Bian, Y., Sell, A., Wei, S., Grove, S., Johnson, J.K., et al. (2022). CD8<sup>+</sup> T cells and fatty acids orchestrate tumor ferroptosis and immunity via ACSL4. *Cancer Cell* 40, 365–378.e6. <https://doi.org/10.1016/j.ccell.2022.02.003>.
  38. Simmons, J.D., Segnitz, R.M., Dill-McFarland, K.A., Stein, C.M., Peterson, G.J., Mayanja-Kizza, H., Boom, W.H., and Hawn, T.R. (2023). Differentially expressed transcript isoforms associate with resistance to tuberculin skin test and interferon gamma release assay conversion. *PLoS One* 18, e0284498. <https://doi.org/10.1371/journal.pone.0284498>.
  39. Phat, N.K., Tien, N.T.N., Anh, N.K., Yen, N.T.H., Lee, Y.A., Trinh, H.K.T., Le, K.M., Ahn, S., Cho, Y.S., Park, S., et al. (2023). Alterations of lipid-related genes during anti-tuberculosis treatment: insights into host immune responses and potential transcriptional biomarkers. *Front. Immunol.* 14, 1210372. <https://doi.org/10.3389/fimmu.2023.1210372>.
  40. Liu, Y., Chen, W., Cen, Y., Zhao, X., Chen, Z., Liang, Y., Huang, Z., He, X., and Yang, G. (2023). Hepatocyte ferroptosis contributes to anti-tuberculosis drug-induced liver injury: Involvement of the HIF-1 $\alpha$ /SLC7A11/GPx4 axis. *Chem. Biol. Interact.* 376, 110439. <https://doi.org/10.1016/j.cbi.2023.110439>.
  41. Wang, J., Zheng, M., Yang, X., Zhou, X., and Zhang, S. (2023). The Role of Cathepsin B in Pathophysiologies of Non-tumor and Tumor tissues: A Systematic Review. *J. Cancer* 14, 2344–2358. <https://doi.org/10.7150/jca.86531>.
  42. Nagakannan, P., Islam, M.I., Conrad, M., and Eftekharpour, E. (2021). Cathepsin B is an executioner of ferroptosis. *Biochim. Biophys. Acta Mol. Cell Res.* 1868, 118928. <https://doi.org/10.1016/j.bbamcr.2020.118928>.
  43. Kuang, F., Liu, J., Li, C., Kang, R., and Tang, D. (2020). Cathepsin B is a mediator of organelle-specific initiation of ferroptosis. *Biochem. Biophys. Res. Commun.* 533, 1464–1469. <https://doi.org/10.1016/j.bbrc.2020.10.035>.
  44. Amaral, E.P., Riteau, N., Moayeri, M., Maier, N., Mayer-Barber, K.D., Pereira, R.M., Lage, S.L., Kubler, A., Bishai, W.R., D'Império-Lima, M.R., et al. (2018). Lysosomal Cathepsin Release Is Required for NLRP3-Inflammasome Activation by Mycobacterium tuberculosis in Infected Macrophages. *Front. Immunol.* 9, 1427. <https://doi.org/10.3389/fimmu.2018.01427>.
  45. Wei, J., Zhang, Y., Li, H., Wang, F., and Yao, S. (2023). Toll-like receptor 4: A potential therapeutic target for multiple human diseases. *Biomed. Pharmacother.* 166, 115338. <https://doi.org/10.1016/j.biopha.2023.115338>.
  46. Li, D., Tian, L., Nan, P., Zhang, J., Zheng, Y., Jia, X., Gong, Y., and Wu, Z. (2023). CerS6 triggered by high glucose activating the TLR4/IKK $\beta$  pathway regulates ferroptosis of LO2 cells through mitochondrial oxidative stress. *Mol. Cell. Endocrinol.* 572, 111969. <https://doi.org/10.1016/j.mce.2023.111969>.
  47. Abel, B., Thieblemont, N., Quesniaux, V.J.F., Brown, N., Mpagi, J., Miyake, K., Bihl, F., and Ryffel, B. (2002). Toll-like receptor 4 expression is required to control chronic Mycobacterium tuberculosis infection in mice. *J. Immunol.* 169, 3155–3162. <https://doi.org/10.4049/jimmunol.169.6.3155>.
  48. Park, J., Kim, H., Kwon, K.W., Choi, H.H., Kang, S.M., Hong, J.J., and Shin, S.J. (2020). Toll-like receptor 4 signaling-mediated responses are critically engaged in optimal host protection against highly virulent Mycobacterium tuberculosis K infection. *Virulence* 11, 430–445. <https://doi.org/10.1080/21505594.2020.1766401>.
  49. Qiu, B., Liu, Q., Li, Z., Song, H., Xu, D., Ji, Y., Jiang, Y., Tian, D., and Wang, J. (2020). Evaluation of cytokines as a biomarker to distinguish active tuberculosis from latent tuberculosis infection: a diagnostic meta-analysis. *BMJ Open* 10, e039501. <https://doi.org/10.1136/bmjopen-2020-039501>.
  50. Qiu, X., Tang, Y., Yue, Y., Zeng, Y., Li, W., Qu, Y., and Mu, D. (2019). Accuracy of interferon- $\gamma$ -induced protein 10 for diagnosing latent tuberculosis infection: a systematic review and meta-analysis. *Clin. Microbiol. Infect.* 25, 667–672. <https://doi.org/10.1016/j.cmi.2018.12.006>.
  51. Namasivayam, S., Kauffman, K.D., McCulloch, J.A., Yuan, W., Thovarai, V., Mittereder, L.R., Trinchieri, G., Barber, D.L., and Sher, A. (2019). Correlation between Disease Severity and the Intestinal Microbiome in Mycobacterium tuberculosis-Infected Rhesus Macaques. *mBio* 10, e01018-19. <https://doi.org/10.1128/mBio.01018-19>.
  52. Mori, G., Morrison, M., and Blumenthal, A. (2021). Microbiome-immune interactions in tuberculosis. *PLoS Pathog.* 17, e1009377. <https://doi.org/10.1371/journal.ppat.1009377>.
  53. Dumas, A., Corral, D., Colom, A., Levillain, F., Peixoto, A., Hudrisier, D., Poquet, Y., and Neyrolles, O. (2018). The Host Microbiota Contributes to Early Protection Against Lung Colonization by Mycobacterium tuberculosis. *Front. Immunol.* 9, 2656. <https://doi.org/10.3389/fimmu.2018.02656>.
  54. Hu, Y., Feng, Y., Wu, J., Liu, F., Zhang, Z., Hao, Y., Liang, S., Li, B., Li, J., Lv, N., et al. (2019). The Gut Microbiome Signatures Discriminate Healthy From Pulmonary Tuberculosis Patients. *Front. Cell. Infect. Microbiol.* 9, 90. <https://doi.org/10.3389/fcimb.2019.00090>.
  55. Hu, Y., Yang, Q., Liu, B., Dong, J., Sun, L., Zhu, Y., Su, H., Yang, J., Yang, F., Chen, X., and Jin, Q. (2019). Gut microbiota associated with pulmonary tuberculosis and dysbiosis caused by anti-tuberculosis drugs. *J. Infect.* 78, 317–322. <https://doi.org/10.1016/j.jinf.2018.08.006>.
  56. Yang, F., Yang, Y., Chen, L., Zhang, Z., Liu, L., Zhang, C., Mai, Q., Chen, Y., Chen, Z., Lin, T., et al. (2022). The gut microbiota mediates protective immunity against tuberculosis via modulation of lncRNA. *Gut Microb.* 14, 2029997. <https://doi.org/10.1080/19490976.2022.2029997>.
  57. (2000). Diagnostic Standards and Classification of Tuberculosis in Adults and Children. This official statement of the American Thoracic Society and the Centers for Disease Control and Prevention was adopted by the ATS Board of Directors, July 1999. This statement was endorsed by the Council of the Infectious Disease Society of America, September 1999. *Am. J. Respir. Crit. Care Med.* 161, 1376–1395. <https://doi.org/10.1164/ajrccm.161.4.16141>.
  58. Langfelder, P., and Horvath, S. (2008). WGCNA: an R package for weighted correlation network analysis. *BMC Bioinf.* 9, 559. <https://doi.org/10.1186/1471-2105-9-559>.

## STAR★METHODS

### KEY RESOURCES TABLE

REAGENT or RESOURCE	SOURCE	IDENTIFIER
<b>Biological samples</b>		
Blood from the patients with active TB and healthy controls	The Eighth Medical Center of PLA General Hospital	N/A
<b>Chemicals, peptides, and recombinant proteins</b>		
Ficoll-Hypaque		Cytiva
Single Cell 3' Reagent Kit V3.1		10× Genomics
<b>Deposited data</b>		
OMIX006478	The Eighth Medical Center of PLA General Hospital	<a href="https://ngdc.cnbc.ac.cn/omix">https://ngdc.cnbc.ac.cn/omix</a>
<b>Software and algorithms</b>		
Cell Ranger (version 7.1.0)	analysis pipelines that process Chromium single cell data	10× Genomics ( <a href="https://www.10xgenomics.com/support/software/cell-ranger">https://www.10xgenomics.com/support/software/cell-ranger</a> )
R (version 4.1.3)	R software	<a href="http://www.R-project.org">http://www.R-project.org</a>
Seurat (version 4.3.0)	R package	<a href="https://satijalab.org/seurat/">https://satijalab.org/seurat/</a>
DoubletFinder (version 2.0.3)	R package	<a href="https://github.com/chris-mcginis-ucsf/DoubletFinder">https://github.com/chris-mcginis-ucsf/DoubletFinder</a>
harmony (version 0.1.1)	R package	<a href="https://github.com/immunogenomics/harmony">https://github.com/immunogenomics/harmony</a>
AUCell (version 1.16.0)	R package	<a href="https://github.com/aertslab/AUCell?tab=readme-ov-file">https://github.com/aertslab/AUCell?tab=readme-ov-file</a>
Mococle (version 2.22.0)	R package	<a href="https://cole-trapnell-lab.github.io/monocle-release/">https://cole-trapnell-lab.github.io/monocle-release/</a>
limma (version 3.50.3)	R package	<a href="https://bioinf.wehi.edu.au/limma/">https://bioinf.wehi.edu.au/limma/</a>
clusterProfiler (version 4.2.2)	R package	<a href="https://github.com/YuLab-SMU/clusterProfiler">https://github.com/YuLab-SMU/clusterProfiler</a>
ConsensusClusterPlus (version 1.58.0)	R package	<a href="https://bioconductor.org/packages/release/bioc/html/ConsensusClusterPlus.html">https://bioconductor.org/packages/release/bioc/html/ConsensusClusterPlus.html</a>
WGCNA (version 1.72-1)	R package	<a href="https://github.com/cran/WGCNA">https://github.com/cran/WGCNA</a>
glmnet (version 4.1-7)	R package	<a href="https://glmnet.stanford.edu/">https://glmnet.stanford.edu/</a>
StepReg (version 1.4.4)	R package	<a href="https://cran.r-project.org/web/packages/StepReg/index.html">https://cran.r-project.org/web/packages/StepReg/index.html</a>
olsrr (version 0.5.3)	R package	<a href="https://github.com/rsquaredacademy/olsrr">https://github.com/rsquaredacademy/olsrr</a>
pROC (v1.18.5)	R package	<a href="https://xrobin.github.io/pROC/">https://xrobin.github.io/pROC/</a>
ggsignif (ggsignif)	R package	<a href="https://github.com/const-ae/ggsignif">https://github.com/const-ae/ggsignif</a>

### RESOURCE AVAILABILITY

#### Lead contact

Further information and requests for resources should be directed to and will be fulfilled by the lead contact, Xiaoxing Cheng (e-mail: [xcheng2@139.com](mailto:xcheng2@139.com)).

#### Materials availability

This study did not generate new unique reagents.

#### Data and code availability

- The data of single-cell sequencing reported in this paper have been deposited in the OMIX, China National Center for Bioinformatics / Beijing Institute of Genomics, Chinese Academy of Sciences (<https://ngdc.cnbc.ac.cn/omix>; accession number: OMIX006478).

- GSE62525, GSE107991, GSE107994, GSE89403, GSE157657 and GSE39941 were downloaded from Gene Expression Omnibus (GEO, <http://www.ncbi.nlm.nih.gov/geo>).
- This paper does not report original code.
- Any additional information required to reanalyze the data reported in this paper is available from the [lead contact](#) upon request.

## EXPERIMENTAL MODEL AND STUDY PARTICIPANT DETAILS

Four patients with active TB and two sex and age-matched healthy controls were recruited in the study. Among the four patients with TB, patient no.1 was a 27 years old female, patient no.2 was an 18 years old female, patient no. 3 was a 28 years old male and patient no. 4 was a 45 years old female. Healthy controls included a 41 years old male and a 25 years old female. All of the patients with TB and healthy controls are ethnic Han Chinese. All patients of TB were diagnosed according to Diagnostic Standards and Classification of Tuberculosis published by the American Lung Association.<sup>57</sup> The study was approved by the Ethics Committee of the Eighth Medical Center of PLA General Hospital and written informed consent was obtained from all participants.

## METHOD DETAILS

### Purification of peripheral blood mononuclear cells (PBMCs)

Anti-coagulated whole blood was obtained from patients with TB and healthy controls and peripheral blood mononuclear cells (PBMCs) were purified by density gradient centrifugation with Ficoll-Hypaque (Cytiva, Marlborough, MA, USA).

### Single-cell library construction

Single-cell suspensions of PBMCs were loaded onto the Chromium™ Single-Cell Controller instrument (10× Genomics, Pleasanton, CA, USA) to generate single-cell gel beads in emulsions. Barcoded single-cell cDNAs were generated by reverse transcription and were amplified to construct scRNA-seq libraries using 10× Genomics Single Cell 3' Reagent Kit V3.1 (10× Genomics). Libraries were sequenced on the Illumina sequencing platform (Novaseq6000) (Illumina, San Diego, CA, USA).

### Single-cell transcriptome data analysis

The unique molecular identifier (UMI) count matrix was processed by the Cell Ranger (v7.1.0). Cells with less than 300 genes, less than 1000 RNA counts, < 5% ribosome gene counts, and > 20% mitochondrial gene counts were removed by R package Seurat (v4.3.0), and doublet were removed by DoubletFinder (v2.0.3). After applying these quality control criteria, 64,336 single cells that remained for inclusion were used for downstream analyses. The filtered digital gene expression matrix was normalized and aggregated using the R package harmony (v0.1.1).

### Principal component analysis and annotation of cell clusters

Principal component analysis was performed to reduce the dimensionality on the log-transformed gene-barcode matrices of the top variable 2000 genes. The number of principal components was 40 and resolution was 1.0. Cells were clustered based on a graph-based clustering approach in the FindNeighbors and FindClusters functions and visualized in two dimensions using the t-distributed stochastic neighbor embedding (t-SNE) method with R package Seurat (v4.3.0). Cell types were annotated according cell markers from the FindAllMarkers function of Seurat.

### Ferroptosis-related gene scoring

Ferroptosis-related gene list was obtained from the FerrDb database (<http://www.zhounan.org/ferrdb/>).<sup>22</sup> Cells were scored using R package AUCell (1.16.0). "AUCell-explore threshold" was used to determine the threshold. If AUC was above the threshold, the gene set was considered to be activated.

### Pseudotime analysis

Pseudotime analysis was performed by R package Mococle (v2.22.0). Myeloid cells clusters were extracted and projected into different cell clusters based on different cell marker genes. DDRTree approach was utilized to reduce the dimension and orderCell was used to determine cell differentiation states.

### Dataset collection and processing

The gene expression datasets of GSE62525, GSE107991, GSE107994, GSE39941, GSE89403 and GSE157657 were downloaded from Gene Expression Omnibus (GEO, <http://www.ncbi.nlm.nih.gov/geo>). These datasets were selected in the study because they investigate blood transcriptional expression in patients with TB and controls. PBMCs samples from 14 patients with TB, 14 individuals with latent TB infection (LTBI) and 14 healthy controls (HC) were included in GSE62525. Whole blood samples from 21 patients with TB, 21 individuals with LTBI and 13 HC were included in GSE107991. GSE107994 contained whole blood samples from 53 patients with TB, 49 individuals with LTBI and 50 HC.

GSE39941 has 68 LTBI, 190 patients with TB and 233 patients with other diseases. Dataset GSE89403 included 50 HC, 142 cured patients with TB and 14 patients with failed anti-TB treatment. GSE157657 contained 38 healthy controls and 45 patients with TB.

### Identification of differentially expressed genes (DEGs) and gene ontology enrichment analysis

R package limma was applied to identify the DEGs among patients with TB, LTBI and HC in GSE62525, with the filtering threshold setting of adjusted p-value  $\leq 0.05$  and  $|\log_2$  fold change (FC)|  $\geq 1$ . R package ClusterProfiler was exploited to perform Gene Ontology (GO) enrichment analysis based on the DEGs between patients with TB and LTBI or HC. Enriched GO pathways were determined according to the cut-off criterion of adjusted p-value  $\leq 0.05$ .

### Consensus clustering analysis

Human immune-related gene sets were obtained from ImmPort and InnateDB databases.<sup>23,24</sup> The R package ConsensusClusterPlus(v1.58.0) was used to perform consensus clustering analysis to investigate the association between immune-related genes and the disease states, with the maximum number of clusters set at 6.

### Weighted gene co-expression network analysis

Weighted gene co-expression network analysis (WGCNA) is a well-established method for studying biological networks and diseases.<sup>58</sup> Thus, WGCNA was performed with the R package WGCNA(1.72-1) to identify key modules related to TB by using immune-related genes in GSE62525 dataset. Correlation of the modules and gene significance of active TB were determined.

### Screening of ferroptosis-related genes with diagnostic value by machine learning algorithms

Three machine learning algorithms, LASSO (Least Absolute Shrinkage and Selection Operator), Stepwise Regression and All Subset Regression, were used in the study. LASSO regression analysis was performed by R package "glmnet", Stepwise Regression with "StepReg"(v1.4.4) and All Subset Regression with the R package "olsrr"(v0.5.3). The datasets from GSE62525, GSE107991, GSE107994 and GSE39941 were used to assess the diagnostic value of the 3 bub genes by calculating the AUC with R package "pROC" (v1.18.5).

### QUANTIFICATION AND STATISTICAL ANALYSIS

Unpaired Wilcoxon test was used for statistical analysis with R package "ggsignif". Pearson correlation analysis was used to calculate correlation coefficient. Test was two-tailed and  $p < 0.05$  was considered significant.